Maximum amplitude of the high-redshift 21-cm absorption feature

Pablo Villanueva-Domingo,[1,*] Olga Mena,[1,†] and Jordi Miralda-Escudé[2,3,‡]

[1]*Instituto de Física Corpuscular (IFIC), CSIC-Universitat de Valencia, Apartado de Correos 22085, E-46071 Paterna, Spain*

[2]*Institut de Ciències del Cosmos, Universitat de Barcelona (IEEC-UB), E-08028 Barcelona, Spain*

[3]*Institució Catalana de Recerca i Estudis Avançats, E-08010 Barcelona, Spain*

(Received 7 January 2020; accepted 12 March 2020; published 3 April 2020)

We examine the maximum possible strength of the global 21-cm absorption dip on the cosmic background radiation at high-redshift caused by the atomic intergalactic medium, when the Lyman-α coupling is maximum, assuming no exotic cooling mechanisms from interactions with dark matter. This maximum absorption is limited by three inevitable factors that need to be accounted for: (a) heating by energy transferred from the cosmic background radiation to the hydrogen atoms via 21-cm transitions, dubbed as *21-cm heating*; (b) Lyα heating by scatterings of Lyα photons from the first stars; (c) the impact of the expected density fluctuations in the intergalactic gas in standard cold dark matter theory, which reduces the mean 21-cm absorption signal. Inclusion of this third novel effect reduces the maximum global 21-cm absorption by ∼10%. Overall, the three effects studied here reduce the 21-cm global absorption by ∼20% at $z \simeq 17$.

DOI: 10.1103/PhysRevD.101.083502

I. INTRODUCTION

The first nonlinear structures containing baryonic matter in the Universe are expected to form in the cold dark matter (CDM) model of structure formation at redshift $z \sim 20$, when the intergalactic medium (IGM) was mostly atomic and had been adiabatically cooling since the residual electrons left over from recombination could no longer keep the temperature equal to that of the cosmic background radiation (CBR). The resulting temperature was $\bar{T}_{\rm ad} \simeq 8\ {\rm K}[(1+z)/20]^2$ (e.g., [1]), which implies a comoving Jeans scale for the atomic gas [with adiabatic sound speed $c_s^2 = 5k_B\bar{T}_{\rm ad}/(3\mu m_p)$, where μ is the mean molecular weight and m_p the mass of the proton] of

$$\lambda_J = \frac{\pi(1+z)}{H(z)}\sqrt{\frac{40k_B\bar{T}_{\rm ad}}{9\mu m_p}} \simeq 9.1\left(\frac{1+z}{20}\right)^{1/2}\ {\rm kpc}, \qquad (1)$$

where $H(z)$ is the Hubble expansion rate. Throughout this paper we use the standard ΛCDM model with $H_0 = 68\ {\rm km\,s^{-1}\,Mpc^{-1}}$, $\Omega_{m0} = 0.308$, and $\Omega_{b0} = 0.048$, see e.g., [2].

There is a strong interest in cosmology in detecting density fluctuations of the IGM at this early epoch, because they are probing the smallest scales of primordial fluctuations that can be detected, and the conditions that gave rise to the formation of the first stars in the Universe (e.g., [3]). Absorption of the CBR radiation in the redshifted 21-cm hyperfine line of atomic hydrogen offers the most plausible method to detect this primitive and coldest state of baryonic matter.

Experiments targeting a measurement of the cosmological 21-cm line, arising from spin-flip transitions between the triplet and the ground singlet states in neutral hydrogen in the IGM, open a new window to the epochs of reionization and the dark age of the Universe. In particular, observation of 21-cm absorption at high redshift probes the epoch when light from the first stars, which had not yet ionized or heated the IGM, was able to couple the spin and kinetic temperatures of the atomic hydrogen through the Wouthuysen-Field effect [4,5]. Although initial studies suggested that 21-cm absorption might be swamped by rapid heating of the IGM, and the corresponding 21-cm emission, by the same Lyα photons responsible for the spin and kinetic temperature couplings (the Lyα heating effect [6]), this heating was shown to be small and to allow for an extended epoch of 21-cm absorption if heating caused by x-ray emission of the first stars is not very strong [7–10]. This offers promising prospects for 21-cm observations of the primitive, cold atomic medium, as a probe to primordial mass fluctuations at very small scales.

A number of observatories aim to detect the 21-cm cosmological line. An early result by the experiment to detect the global epoch of reionization signature (EDGES) [11] claimed a 21-cm absorption temperature at a redshift $z \sim 17$ twice larger than the maximum allowed one in the

*pablo.villanueva@ific.uv.es
†olga.mena@ific.uv.es
‡miralda@icc.ub.edu

absence of any heating, and for the baryon density derived from CBR fluctuations and primordial nucleosynthesis [12]. Many studies explored exotic scenarios of strong interactions of baryons with dark matter that might further cool the early atomic IGM [13–15], but the EDGES result is likely affected by foregrounds or systematics [16–18]. Other high-redshift 21-cm searches include the future large-aperture experiment to detect the dark ages (LEDA) [19], and the moon orbiting space observatory dark ages radio-experiment (DARE) [20].

To help interpret future results of the 21-cm cosmological signal, it is useful to derive the maximum possible global 21-cm absorption in standard cosmology, taking into account and accurately including any effects that may impact the average amplitude of the absorption. This is the goal of the present study, which examines relevant astrophysical effects at the epoch of interest that may substantially modify the global 21-cm absorption dip. Although many calculations and models have been done (see e.g., [21] for an analytical estimation taking into account inhomogeneous distributions of the gas), we include here a comprehensive study of the global effect of baryon density fluctuations, whose impact has not been analyzed from an analytical perspective in the literature.

The structure of the paper is as follows. We review in Sec. II the basics of the 21-cm global signal, discussing the imprint of Lyα emission and heating sources. Section III describes the effect of IGM density fluctuations on the global signal. Results are presented in Sec. IV, accounting separately for each heating contribution first, and then illustrating the final 21-cm absorption amplitude including all effects. We conclude in Sec. V.

II. THE 21-CM SIGNAL

The 21-cm emission and absorption signal arises from the population of the singlet and triplet states of the atomic hydrogen hyperfine structure, n_0 and n_1 respectively, governed by the spin temperature T_S through the relation $n_1/n_0 = 3\exp(-T_*/T_S)$, with $T_* = h\nu_0 = 0.0682$ K. The differential brightness temperature in 21-cm absorption can be written as [1,22]

$$\delta T_b(\Delta) = T_0 \Delta \left(1 - \frac{T_\gamma}{T_S(\Delta)}\right), \tag{2}$$

where T_γ is the CMB photon temperature, $\Delta = 1 + \delta = \rho/\bar{\rho}$ is the gas density divided by its mean value, $T_0 = 27 x_{\rm HI}\sqrt{(1+z)/10}$ mK is the global emission temperature at the mean density for the cosmological model we use when $T_S \gg T_\gamma$, and $x_{\rm HI}$ the neutral hydrogen fraction.[1]

[1]The 21-cm signal is also affected by peculiar velocity gradients, but in the optically thin regime the mean value is not affected because peculiar velocities only redistribute the absorption over frequency.

In this work we focus on the epoch prior to reionization, setting $x_{\rm HI} \simeq 1$. The spin temperature T_S evolution is determined by various energy exchange processes: (i) absorption and emission of CMB photons, coupling T_S to T_γ; (ii) collisions with electrons, protons or other H atoms, coupling T_S to the gas kinetic temperature T_K; and (iii) the Wouthuysen-Field mechanism [4,5], i.e., Lyα photon scattering, coupling T_S to the *color* radiation temperature T_α, which measures the slope of the radiation background spectrum near the center of the Lyα line where most of the scatterings occur. The spin temperature is rapidly set to an equilibrium between these processes determined by the equation

$$T_S^{-1} = \frac{T_\gamma^{-1} + x_c T_K^{-1} + x_\alpha T_\alpha^{-1}}{1 + x_c + x_\alpha}, \tag{3}$$

where x_c and x_α are coupling coefficients for collisions and Lyα scattering, respectively. In general, we can safely assume that $T_\alpha \simeq T_K$ [1,22]. We make use of the fits from [23,24] for x_c, although coupling by collisions is important only at high redshifts. The coupling after star formation has started is driven therefore by Lyα scattering,

$$x_\alpha = \frac{16\pi^2 T_* e^2 f_{12}}{27 A_{10} T_\gamma m_e c} S_\alpha J_\alpha, \tag{4}$$

where f_{12} is the oscillator strength of the Lyα transition, A_{10} the spontaneous decay rate, m_e the electron mass of the electron, e the charge of the electron, c the speed of light, S_α is an order unity correction factor accounting for the detailed shape of the spectrum near the resonance, and J_α is the photon Lyα flux per unit frequency at the Lyα line center. We adopt the wing approximation for S_α obtained in [9]. We now explain how the evolution of the two crucial quantities for 21-cm absorption, the Lyα flux J_α and the kinetic temperature T_K, are obtained.

A. Lyα flux

The Lyα flux from direct stellar emission of UV photons, $J_{\alpha\star}$, is given by the sum over the Ly-n levels which can lead to a $2p \to 1s$ transition through a decaying cascade. Photons redshifting to a Lyman resonance are always absorbed owing to the high optical depth of the IGM. Photons reaching the Ly-n resonance at redshift z have to be emitted at a redshift below $1 + z_{{\rm max},n} = (1+z)[1-(n+1)^{-2}]/[1-n^{-2}]$. Defining the probability to generate a Lyα photon after absorption by the n level as recycled fraction of level n, $f_{\rm rec}(n)$ [25], the total Lyα flux can be written in terms of the photon comoving emissivity $\epsilon_\alpha(\nu, z)$ as

$$J_\alpha = \frac{c(1+z)^2}{4\pi} \sum_{n=2}^{n_{\rm max}} f_{\rm rec}(n) \int_z^{z_{{\rm max},n}} dz' \frac{\epsilon_\alpha(\nu'_n, z')}{H(z')}, \tag{5}$$

where the emission frequency is $\nu'_n = \nu_n(1+z')/(1+z)$, $\nu_n = \nu_{LL}(1-n^{-2})$, ν_{LL} is the Lyman limit frequency and $H(z)$ is the Hubble expansion rate.

We use a simple model for the emissivity, based on a constant emission per unit mass of collapsed halos above a minimum mass $M_{\rm min}$, at the moment mass is added to them [26],

$$\epsilon_\alpha(\nu, z) = \varepsilon(\nu) f_* \bar{n}_{b,0} \frac{df_{\rm coll}(z)}{dt}, \tag{6}$$

where f_* is the fraction of baryons that form stars when new mass is added to collapsed halos, and $\bar{n}_{b,0}$ is the mean comoving baryon number density. We take $f_* = 0.01$ following previous works on radiation-hydrodynamic simulations of high-redshift galaxies (e.g., [27]) or on the comparison of the star formation rate density to the one derived from UV luminosity function measurements [28]. The fraction of mass collapsed in halos which host star formation $f_{\rm coll}$ is

$$f_{\rm coll}(z) = \frac{1}{\rho_m} \int_{M_{\rm min}(z)}^{\infty} dM\, M \frac{dn}{dM}, \tag{7}$$

where $\frac{dn}{dM}$ is the halo mass function, computed here using the Sheth-Tormen function [29,30]. The minimum mass $M_{\rm min}$ is fixed here to the virial mass corresponding to a halo virial temperature of $T_{\rm vir} = 10^4$ K. This neglects star formation that can occur at lower virial temperatures via molecular cooling, and assumes that most of the emissivity is due to stellar populations formed when atomic hydrogen cooling of partially ionized matter is already important. In any case, Eq. (7) is only a simple but reasonable model for the evolution of the emissivity from first galaxies. The radiation spectral distribution, $\varepsilon(\nu)$, is normalized to $\int_{\nu_\alpha}^{\nu_{LL}} d\nu \varepsilon(\nu) = N_{\rm tot} \simeq 9690$, using the total number of photons emitted between the Lyα and the Lyman limit, $N_{\rm tot}$, from the population II (or low-metallicity) model of [26]. Given the uncertainty in the specific spectral shape, we assume an emissivity proportional to ν^{-1}, resulting in the normalization $\varepsilon(\nu) = N_{\rm tot}/\ln(4/3)\nu^{-1}$. All in all, the Ly$\alpha$ flux is

$$J_\alpha = \frac{c(1+z)^3 f_* \bar{n}_{b,0} N_{\rm tot}}{4\pi \nu_\alpha ln(4/3)} \times \sum_{n=2}^{n_{\rm max}} f_{\rm rec}(n) \frac{\nu_\alpha}{\nu_n} (f_{\rm coll}(z) - f_{\rm coll}(z_{{\rm max},n})), \tag{8}$$

with $\nu_\alpha = \nu_2$ the Lyα frequency. This flux differs by less than 10% from the one computed with the more complex model of a piecewise power-law spectrum presented in [26].

B. Heating sources

The kinetic temperature T_K can be determined by solving the thermal evolution equation,

$$\frac{dT_K}{dt} + 2HT_K - \frac{2}{3}\frac{T_K}{\Delta}\frac{d\Delta}{dt} + \frac{T_K}{1+x_e}\frac{dx_e}{dt} = \frac{2\mathcal{Q}}{3n_b(1+x_e)}, \tag{9}$$

where x_e is the ionized fraction left over from recombination ($x_e \sim 10^{-4}$), $n_b = \bar{n}_{b,0}(1+z)^3\Delta$ is the baryon number density and $\mathcal{Q}$ is the total heating rate per unit volume.

The expected dominant heating mechanism is x-ray heating from astrophysical sources (e.g., [31]). We also account for two other usually neglected model-independent heating sources: CMB photons causing 21-cm transitions and Lyα scatterings. Compton cooling is also taken into account, although it is negligible due to the small ionized fraction in the IGM prior to reionization.

(i) *21-cm heating*:

The heating rate due to absorption and emission of CMB photons by the hyperfine levels was derived in [10] and can be written as

$$\mathcal{Q}|_{21} = \frac{3}{4} n_H x_{\rm HI} x_{\rm CMB} A_{10} T_* \left(\frac{T_\gamma}{T_S} - 1\right), \tag{10}$$

where $n_H = \bar{n}_{H,0}(1+z)^3\Delta$ is the number density of hydrogen, $\bar{n}_{H,0}$ is its comoving average, and $x_{\rm CMB} = (1-e^{-\tau_{21}})/\tau_{21} \simeq 1$, where the 21-cm optical depth τ_{21} is small.

(ii) Lyα *heating*

Another heating source is Lyα scattering which, following [7,9], has a contribution from continuous and injected photons (photons that redshift into the Lyα resonance from the continuum, or are produced at the Lyα resonance after absorption at a higher energy line, respectively) of

$$\mathcal{Q}|_{{\rm Ly}\alpha,{\rm k}} = \frac{4\pi H h \nu_\alpha \Delta\nu_D}{c} J_{\infty,k} I_k, \tag{11}$$

where k stands for $k = c$, *continuous*, or $k = i$, *injected*, with $\Delta\nu_D = \nu_\alpha\sqrt{2k_B T_K/(m_p c^2)}$ the Doppler broadening parameter. The integrals I_c and I_i encode the details on the scattering effects and depend on the temperature and the Gunn-Peterson optical depth $\tau_{\rm GP}$ (the optical depth of Lyα photons redshifting through the IGM). For these quantities, we use the fits provided by [9].

(iii) *X-ray heating*

The heating from astrophysical x-ray sources is accounted for with the on-the-spot approximation (e.g., [31]),

$$\mathcal{Q}|_X = \xi_X \epsilon_X f_* f_{\rm heat} \mu m_p n_b \frac{df_{\rm coll}}{dt}, \tag{12}$$

where we compute the fraction of energy from x rays that is converted to heat in the IGM, $f_{\rm heat}$, using the fit from [32]. The fiducial value for the luminosity of the x-ray emission per unit star formation rate is $\epsilon_X = 3.4 \times 10^{40}$ erg s^{-1} $M_\odot^{-1}$ yr, from [31], which is measured from local starburst galaxies. The efficiency parameter ξ_X accounts for deviations from this fiducial value, so in the default model, $\xi_{\rm X} = 1$.

III. IGM DENSITY DISTRIBUTION

The mean 21-cm absorption can be affected by the presence of spatial density fluctuations in the atomic gas density of the IGM, ρ. We define the nonlinear probability distribution function (PDF) of the gas density, $P(\Delta)$, where $\Delta = 1 + \delta = \rho/\bar{\rho}$. While the original linear distribution is described by a Gaussian, the PDF becomes non-Gaussian when fluctuations at the Jeans scale of the atomic IGM reach nonlinearity. The probability and mass normalization imply that

$$\int_0^\infty d\Delta P(\Delta) = 1, \qquad \int_0^\infty d\Delta\, \Delta P(\Delta) = 1. \quad (13)$$

In the following, we denote the average of any function f over the density distribution as

$$\langle f \rangle = \int_0^\infty d\Delta\, f(\Delta) P(\Delta), \quad (14)$$

and the second central moment of the distribution, or variance, as $\sigma_\delta^2 = \langle (\Delta - 1)^2 \rangle = \langle \delta^2 \rangle$. We use $\bar{f}$ for the background values, when $\delta = 0$, which, in general, will differ from the value of $\langle f \rangle$.

As a fit to the nonlinear density distribution, the following probability distribution (named in what follows as MHR00) was proposed to fit numerical simulation results by [33],

$$P_{\rm MHR00}(\Delta) = A\Delta^{-\beta} \exp\left[-\frac{(\Delta^{-2/3} - C_0)^2}{2(2\delta_0/3)^2}\right], \quad (15)$$

where A, β, C_0 and δ_0 are free parameters constrained by the normalization conditions in Eq. (13). Figure 1 depicts the MHR00 PDF for three different redshifts. This distribution is motivated to describe the evolution of low-density regions, where gravitational tides are usually small and test particles move away from each other at roughly constant velocity. Therefore, densities decrease as $\rho \sim t^{-3} \sim a^{-9/2}$ in a matter dominated universe and consequently, $\Delta = \rho/\bar{\rho} \sim a^{-3/2}$. Since the linear density field grows as $\delta_l \propto a$, we can write $\Delta \sim \delta_l^{-3/2}$. Therefore, an initial Gaussian distribution in δ_l gives rise to a Gaussian PDF in $\Delta^{-2/3}$, as in Eq. (15). In the linear regime limit, when $\delta_0 \ll 1$, a Gaussian distribution with dispersion δ_0 and $C_0 = 1$ is recovered. For high densities, $\Delta \gg 1$, the probability distribution tends to a power law, $P_{\rm MHR00} \propto \Delta^{-\beta}$. This is easily seen to correspond to a power-law density profile in collapsed objects $\Delta \propto r^{-3/(\beta-1)}$. For our numerical model, we choose $\beta = 5/2$ which corresponds to isothermal halos with overdensity $\Delta \propto r^{-2}$. This distribution was seen to provide a reasonable fit to the results of numerical hydrodynamic simulations for the evolution of a photoionized IGM, simulating the Lyα forest, in Ref. [33].

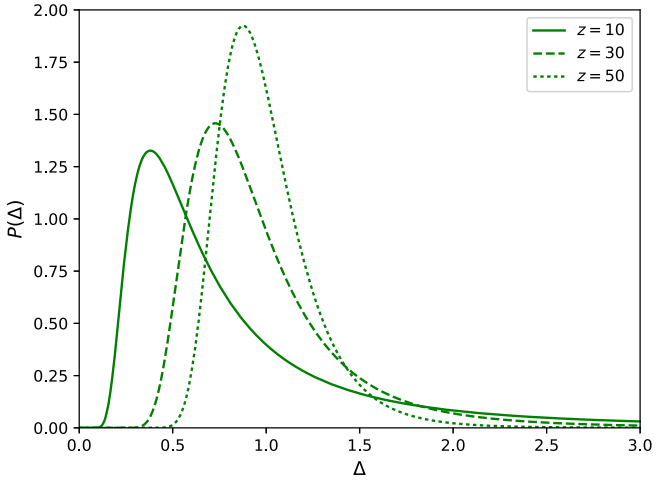

FIG. 1. MHR00 probability distribution of the IGM density for three different redshifts.

For the dispersion of the PDF, we compute a filtered variance from the linear power spectrum using a top-hat sphere of comoving radius R_J as filter,

$$\sigma_l^2(R) = \int \frac{d^3k}{2\pi} P(k) |W(kR_J)|^2. \quad (16)$$

The natural smoothing length for the gas density is the Jeans length at the temperature of the atomic medium, which sets the scale where the collapse of the first halos with high gas overdensities is expected. We use a top-hat filtering radius $R_J = \lambda_J/4$, with the Jeans length λ_J defined in Eq. (1), fixing therefore $\delta_0 = \sigma_l(R_J)$. This roughly corresponds to the scale of the first nonlinear collapse followed by the atomic gas, because the top-hat diameter corresponds to half the full critical wavelength for Jeans instability (the region where the density perturbation is positive). The mass enclosed in a sphere of radius R_J is also close to the Bonnor-Ebert critical gas mass for gravitational instability [34].

Finally, we set an upper cutoff to the distribution at $\Delta_{\rm max} = 10$, fixing the probability distribution to zero at $\Delta > \Delta_{\rm max}$. This is reasonable when the mass fraction that has collapsed on scales substantially larger than R_J is very small, because the atomic gas does not cool effectively and behaves adiabatically, so it cannot collapse to high densities on halos formed from scales comparable to R_J. The values

of the parameters A and C_0 are then determined by the normalization conditions of Eq. (13).

Other choices for the PDF can be considered, such as the log-normal distribution (e.g., [35,36]). We have checked our results for this other distribution, finding no strong dependence on the shape of the PDF of Δ as long as the characteristic width of the distribution is kept fixed.

IV. IMPACT OF IGM DENSITY FLUCTUATIONS ON THE 21-CM SIGNAL

We now present how the 21-cm absorption is affected by the presence of density fluctuations in the atomic IGM, in various models for the heating sources described above and for the Lyα radiation coupling the spin and kinetic temperatures. We have developed our own numerical implementation as a PYTHON code,[2] which solves the thermal evolution accounting for density fluctuations and the various heating terms. Other codes are available in the literature to compute the 21-cm global signature. For instance, the program 21cmFAST [37] computes the space-dependent 21-cm signal from a 3D data cube of the density field, therefore accounting for the impact of the density fluctuations automatically. Our procedure, on the other hand, accounts for density fluctuations analytically to compute the global signal. Another often used code is ARES [38], which computes the global signal with a more realistic radiative transfer calculation of the x-ray heating compared to our on-the-spot approximation of Eq. (12), but does not take into account density fluctuations.

A. Strong Lyα coupling in adiabatic cooling regime

As a first illustrative case, we consider the regime of perfect spin and kinetic temperature coupling by Lyα scattering, while neglecting all heating terms. Therefore, $x_\alpha \gg 1$ and $T_S = T_K$ [see Eqs. (2) and (3)]. This scenario represents the case of a very fast transition to strong coupling before there is any time for substantial heating, so the maximum 21-cm absorption is produced. If the gas cools adiabatically from high redshift in the absence of any heating, the kinetic temperature of the monoatomic gas is related to density as $T_K = \bar{T}_{\rm ad}\Delta^{2/3}$ [see Eq. (9)], where $\bar{T}_{\rm ad} \propto a^{-2}$ is the kinetic temperature at $\Delta = 1$, or $\delta = 0$. The mean background 21-cm emission is

$$\overline{\delta T_b} = T_0\left(1 - \frac{T_\gamma}{\bar{T}_{\rm ad}}\right). \tag{17}$$

The 21-cm background signal is obtained by averaging Eq. (2) over all densities with the strong coupling assumption, $T_S(\Delta) = T_K(\Delta)$:

[2]The PYTHON code used for the calculations is made publicly available at https://github.com/PabloVD/21cmSolver.

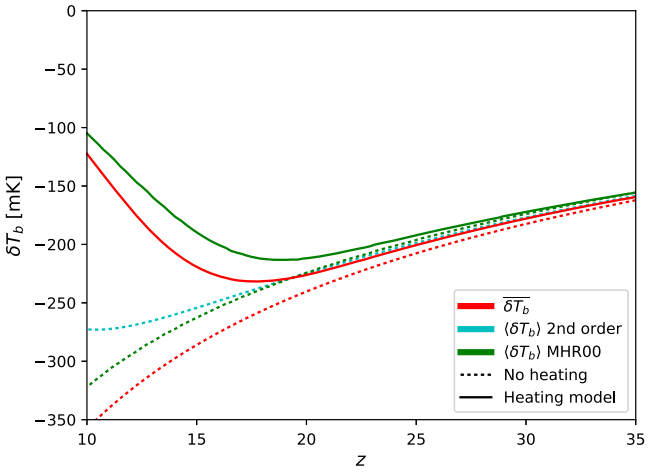

FIG. 2. 21-cm global brightness temperature in the strong Lyα coupling regime at the mean density $\Delta = 1$ (red), and the mean value $\langle\delta T_b\rangle$ accounting for density fluctuations using the second-order approximation of Eq. (20) (cyan), or the MHR00 distribution (green). Dotted lines are for adiabatic cooling while solid lines include 21-cm and Lyα heating terms in our model.

$$\langle\delta T_b\rangle = T_0\left\langle\Delta\left(1 - \frac{T_\gamma}{\bar{T}_{\rm ad}\Delta^{2/3}}\right)\right\rangle = T_0\left(1 - \frac{T_\gamma}{\bar{T}_{\rm ad}}\langle\Delta^{1/3}\rangle\right) \tag{18}$$

$$= \overline{\delta T_b} + T_0\frac{T_\gamma}{\bar{T}_{\rm ad}}(1 - \langle\Delta^{1/3}\rangle) \tag{19}$$

$$= \overline{\delta T_b} + \frac{1}{9}T_0\frac{T_\gamma}{\bar{T}_{\rm ad}}\sigma_\delta^2 + O(\delta^3), \tag{20}$$

where the last equation is valid up to second order in δ, and results from expanding $\langle(1+\delta)^{1/3}\rangle$ in moments of the δ distribution. The impact of density fluctuations is a positive quantity at the second order, added to the global signal, diminishing therefore the maximum possible absorption.

Figure 2 compares the mean absorption 21-cm signal without density fluctuations $\delta\bar{T}_b$ (dotted red line), to $\langle\delta T_b\rangle$ computed from the second order approximation of Eq. (20) (dotted cyan), and to the same mean signal computed from the full MHR00 PDF (dotted green). In the latter case, we use also Eq. (19), which is highly accurate in the absence of the heating terms discussed in Sec. II because the normalized density Δ varies appreciably only when Compton heating of the atomic IGM by the CMB is already small. As expected, density fluctuations imply a lower absorption amplitude by ∼10%, and the second order approximation is close to the exact PDF calculation, deviating substantially only at $z \lesssim 15$.

B. Inclusion of 21-cm and Lyα heating

We now use the simple model of heating sources presented in Sec. II to investigate the impact of the

small-scale density fluctuations in the atomic IGM on the 21-cm absorption evolution as the IGM temperature is increased. As an illustrating exercise, we first maintain the assumption of a perfect coupling of the spin and kinetic temperatures [therefore ignoring the Lyα emissivity discussed in Sec. II and assuming the limit of large x_α in Eq. (3)], but include the heating derived from the Lyα flux and the CMB heating. This is of course not a physically consistent model but it simply allows us to visualize the impact of heating separately from that of the spin and kinetic temperature coupling. The red solid line in Fig. 2 is the result without density fluctuations. For this model, the maximum absorption is reached at $z_{\rm max} \simeq 17$.

We then include the density fluctuations using the model MHR00, using the following simplification: we solve Eq. (9) for a grid of many values of Δ, neglecting the term $d\Delta/dt$. We start the calculation at $z_i = 35$ (at an epoch before there is any significant heating), assuming the initial relation $T(z_i, \Delta) = \bar{T}_{\rm ad}(z_i)\Delta^{2/3}$, we evolve the temperature at each Δ as a function of redshift, and then we compute the mean absorption using the exact equation,

$$\langle \delta T_b \rangle = T_0 \left(1 - \left\langle \Delta \frac{T_\gamma}{T_S(\Delta)} \right\rangle \right). \tag{21}$$

Our justification for neglecting the term $d\Delta/dt$ is that the heating sources increase rapidly with time, so that when evaluating the mean absorption at any redshift z, most of the heating affecting $T_K(z)$ has occurred over a brief time just before redshift z. Taking into account the term $d\Delta/dt$ is complex, because at second order the evolution of Δ is no longer local and one has to compute an average over evolutionary histories of volume elements in the IGM. Furthermore, at high Δ shock heating will inevitably occur in the nonlinear regime. While a number of approximations may be considered for this term, the results would not change dramatically because of the rapid rise of heating sources from the collapse of high-σ halos.

The result when we include only 21-cm and Lyα heating (with no x rays) is shown as the green solid line in Fig. 2, showing the same decrease of the absorption amplitude ($\sim$30 mK at $z \lesssim 18$) compared to the red solid line, and a shift of the redshift of maximum absorption to $z_{\rm max} \simeq 19$. There is therefore a substantial and measurable impact of the IGM small-scale density fluctuations on the global 21-cm absorption history, although the details of the variation of $\delta\bar{T}_b$ with redshift depend on the heating history.

Next, we include the correct Lyα coupling from the model described in Sec. II to calculate the evolution of the spin temperature. In the adiabatic cooling case, we can write analytically the background 21-cm brightness temperature as

$$\overline{\delta T_b} = T_0 \frac{x_{\rm tot}}{1 + x_{\rm tot}} \left(1 - \frac{T_\gamma}{\bar{T}_{\rm ad}}\right), \tag{22}$$

where $x_{\rm tot} = x_\alpha + x_c$. When the Ly$\alpha$ flux, assumed to be homogeneous and independent of the density Δ, dominates the coupling in Eq. (3), then $x_{\rm tot} \simeq x_\alpha$. As before, the mean 21-cm brightness can be approximated to second order in δ, yielding

$$\langle \delta T_b \rangle \simeq \overline{\delta T_b} + \frac{1}{9} T_0 \frac{T_\gamma}{\bar{T}_{\rm ad}} \frac{x_{\rm tot}}{1 + x_{\rm tot}} \sigma_\delta^2. \tag{23}$$

The results using this formula, together with the numerical integration using the full PDF, are depicted with dotted lines in Fig. 3. The dotted lines (no heating) now show a rapid increase of the absorption signal with time because of the rising Lyα intensity, with coupling becoming effective only at $z \lesssim 20$. The inclusion of heating (solid lines in Fig. 3) now produces a reduced absorption with a maximum delayed to $z_{\rm max} \simeq 15$, because of the imperfect coupling, and the presence of density fluctuations also causes as before a further reduced absorption amplitude, of the order of $\sim$15% respect to the background case.

C. General Lyα coupling with heating sources

Finally, Fig. 4 shows the calculated mean 21-cm brightness when x-ray heating is included according to Eq. (12), assuming the three different values of the x-ray efficiency $\xi_X = (0.1, 1, 10)$. For an x-ray emissivity comparable to local starbursts, the maximum 21-cm absorption is reduced from $\sim$140 to $\sim$80 mK, with a shift to a higher maximum redshift $z_{\rm max} \simeq 18$. With $\xi_X = 0.1$ there is only a small reduction in the maximum 21-cm absorption, while with $\xi_X = 10$ the absorption is greatly reduced to a brightness temperature comparable to the 21-cm emission that is already induced by $z \simeq 15$. Of course, the detailed epoch and value of the maximum 21-cm absorption depends on the model we have assumed for the Lyα emission rate as a result of star formation in the earliest, smallest galaxies to form, but the results of this model illustrate how the

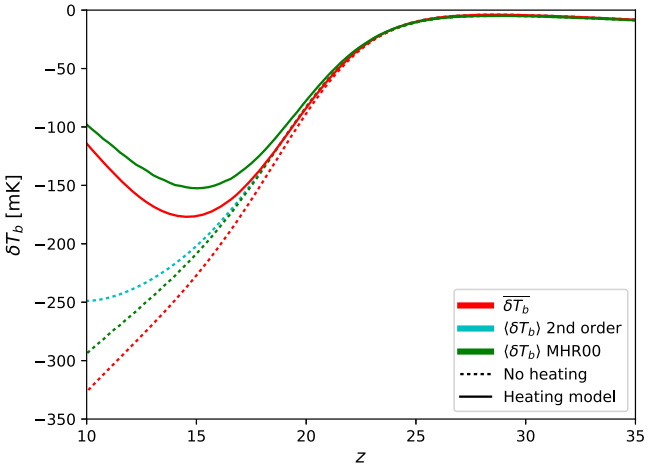

FIG. 3. Same as Fig. 2 but including the correct Lyα coupling to calculate the evolution of the spin temperature.

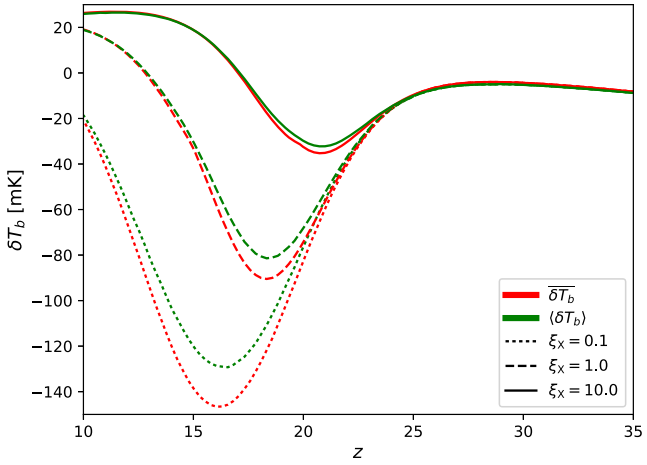

FIG. 4. Same as Fig. 3 but including x-ray heating for three different galaxy emissivities, where $\xi_X = 1$ corresponds to x-ray emission per unit star formation similar to local starbursts.

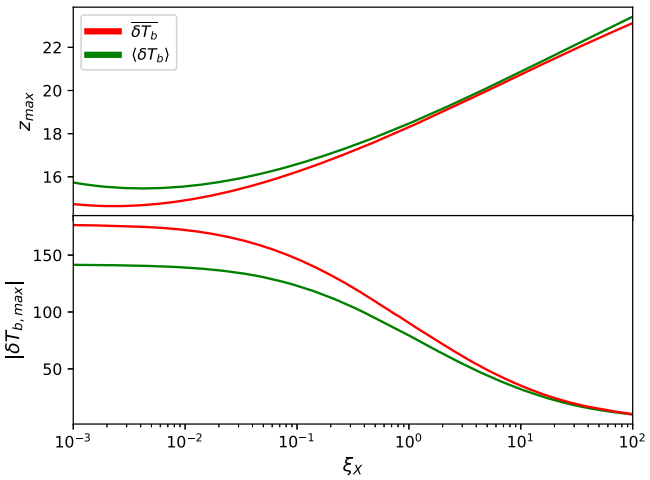

FIG. 5. Maximum absorption $|\delta T_b|$ and redshift when it is reached, as a function of x-ray emission efficiency.

observed 21-cm signal depends on the model and the impact of the small-scale density fluctuations in the atomic IGM. This is shown more clearly in Fig. 5, where the maximum 21-cm absorption δT_b (lower panel) and the redshift $z_{\rm max}$ at which this minimum occurs (upper panel) are plotted as a function of the x-ray efficiency ξ_X, when all three heating sources (21-cm, Lyα and x ray) are included. As before, the red and green curves show the evolution at $\Delta = 1$, and when the density distribution is numerically included as described above. For $\xi_X < 10^{-2}$, x-ray heating is negligible and the maximum possible 21-cm absorption is reached, decreased (in absolute value) by ∼30 mK by the presence of density fluctuations, while for high x-ray emissivity, the absorption amplitude becomes increasingly small and is reached at an increasing redshift.

V. CONCLUSIONS

The properties of the earliest star formation period in the Universe are largely unknown. Understanding this epoch requires detecting matter density fluctuations on tiny scales compared to the galaxy-scale distribution we measure at low redshift, smaller also than the 1 Mpc scales that are probed by the Lyα forest in the spectra of distant quasars. During these primitive stages, the interplay between CMB photons, ultraviolet radiation and atomic hydrogen in the IGM leads to the 21-cm absorption feature in the CMB spectrum. Understanding the depth and redshift location of this absorption feature is crucial to unravel the formation of stars in the first haloes and, ultimately, to probe the nature of dark matter from the small-scale power spectrum. From the observational perspective, the field of 21-cm cosmology is entering a promising era of new data with expectations of first detections in the near future. While numerical simulations are at hand, analytical descriptions of the impact of small-scale density fluctuations in the IGM on the 21-cm absorption profile were missing in the literature. This has been the major goal of this paper: we have discussed how these density fluctuations will significantly reduce the amplitude of the 21-cm absorption peak, and how this absorption reduction depends on the heating sources and the Lyα intensity that determines the coupling of spin and kinetic temperatures. This reduction is not highly dependent on the modeling of the shape of the IGM density distribution, but the expected increase in the distribution breadth due to gravitational evolution ends up producing a nearly constant absorption temperature increase of ∼30 mK at redshifts below the maximum 21-cm absorption, $z < z_{\rm max}$. The shape of the 21-cm absorption dip is highly uncertain, mostly due to the unknown x-ray emission from the first star-forming dwarf galaxies and the Lyα emission determining coupling, but we have shown that the IGM density distribution modifies this absorption dip in a substantial way in any case.

ACKNOWLEDGMENTS

O. M. and P. V. D. are supported by the Spanish Grants No. FPA2017-85985-P and No. SEV-2014-0398 of the MINECO, by PROMETEO/2019/083 and by the European Union Horizon 2020 research and innovation program (Grant Agreements No. 690575 and No. 67489). J. M. was supported in part by Spanish Grants No. AYA2015-71091-P and No. MDM-2014-0369.

[1] J. R. Pritchard and A. Loeb, Rep. Prog. Phys. **75**, 086901 (2012).
[2] P. A. R. Ade *et al.* (Planck Collaboration), Astron. Astrophys. **594**, A13 (2016).
[3] J. B. Muñoz, C. Dvorkin, and F.-Y. Cyr-Racine, arXiv:1911.11144.
[4] S. A. Wouthuysen, Astrophys. J. **57**, 31 (1952).
[5] G. B. Field, Proc. IRE **46**, 240 (1958).
[6] P. Madau, A. Meiksin, and M. J. Rees, Astrophys. J. **475**, 429 (1997).
[7] X.-L. Chen and J. Miralda-Escudé, Astrophys. J. **602**, 1 (2004).
[8] C. M. Hirata, Mon. Not. R. Astron. Soc. **367**, 259 (2006).
[9] S. Furlanetto and J. R. Pritchard, Mon. Not. R. Astron. Soc. **372**, 1093 (2006).
[10] T. Venumadhav, L. Dai, A. Kaurov, and M. Zaldarriaga, Phys. Rev. D **98**, 103513 (2018).
[11] J. D. Bowman and A. E. E. Rogers, Nature (London) **468**, 796 (2010).
[12] J. D. Bowman, A. E. E. Rogers, R. A. Monsalve, T. J. Mozdzen, and N. Mahesh, Nature (London) **555**, 67 (2018).
[13] H. Liu and T. R. Slatyer, Phys. Rev. D **98**, 023501 (2018).
[14] E. D. Kovetz, V. Poulin, V. Gluscevic, K. K. Boddy, R. Barkana, and M. Kamionkowski, Phys. Rev. D **98**, 103529 (2018).
[15] R. Barkana, Nature (London) **555**, 71 (2018).
[16] R. Hills, G. Kulkarni, P. D. Meerburg, and E. Puchwein, Nature (London) **564**, E32 (2018).
[17] R. F. Bradley, K. Tauscher, D. Rapetti, and J. O. Burns, Astrophys. J. **874**, 153 (2019).
[18] P. H. Sims and J. C. Pober, Mon. Not. R. Astron. Soc. **492**, 22 (2020).
[19] L. J. Greenhill and G. Bernardi, arXiv:1201.1700.
[20] J. O. Burns, T. J. W. Lazio, S. D. Bale, J. D. Bowman, R. F. Bradley, C. L. Carilli, S. R. Furlanetto, G. J. A. Harker, A. Loeb, and J. R. Pritchard, Adv. Space Res. **49**, 433 (2012).
[21] Y. Xu, B. Yue, and X. Chen, Astrophys. J. **869**, 42 (2018).
[22] S. Furlanetto, S. P. Oh, and F. Briggs, Phys. Rep. **433**, 181 (2006).
[23] S. Furlanetto and M. Furlanetto, Mon. Not. R. Astron. Soc. **374**, 547 (2007).
[24] B. Zygelman, Astrophys. J. **622**, 1356 (2005).
[25] J. R. Pritchard and S. R. Furlanetto, Mon. Not. R. Astron. Soc. **367**, 1057 (2006).
[26] R. Barkana and A. Loeb, Astrophys. J. **626**, 1 (2005).
[27] J. H. Wise, V. G. Demchenko, M. T. Halicek, M. L. Norman, M. J. Turk, T. Abel, and B. D. Smith, Mon. Not. R. Astron. Soc. **442**, 2560 (2014).
[28] A. Lidz and L. Hui, Phys. Rev. D **98**, 023011 (2018).
[29] R. K. Sheth and G. Tormen, Mon. Not. R. Astron. Soc. **308**, 119 (1999).
[30] R. K. Sheth, H. J. Mo, and G. Tormen, Mon. Not. R. Astron. Soc. **323**, 1 (2001).
[31] S. Furlanetto, Mon. Not. R. Astron. Soc. **371**, 867 (2006).
[32] J. M. Shull and M. E. van Steenberg, Astrophys. J. **298**, 268 (1985).
[33] J. Miralda-Escudé, M. Haehnelt, and M. J. Rees, Astrophys. J. **530**, 1 (2000).
[34] B. T. Draine, *Physics of the Interstellar and Intergalactic Medium* (Princeton University Press, Princeton, NJ, 2011).
[35] P. Coles and B. Jones, Mon. Not. R. Astron. Soc. **248**, 1 (1991).
[36] G. D. Becker, M. Rauch, and W. L. W. Sargent, Astrophys. J. **662**, 72 (2007).
[37] A. Mesinger, S. Furlanetto, and R. Cen, Mon. Not. R. Astron. Soc. **411**, 955 (2011).
[38] J. Mirocha, Mon. Not. R. Astron. Soc. **443**, 1211 (2014).